Scanless two-photon excitation of channelrhodopsin-2

Eirini Papagiakoumou, Francesca Anselmi, Aurélien Bègue, Vincent de Sars, Jesper Glückstad, Ehud Isacoff, Valentina Emiliani

Scanless two-photon excitation of channelrhodopsin-2

Eirini Papagiakoumou, Francesca Anselmi, Aurelien Begue, Vincent de Sars, Jesper Glückstad, Ehud Y Isacoff & Valentina Emiliani

Supplementary Figure 1	Intensity distribution in GPC and DH generated light patterns.
Supplementary Figure 2	Intensity and phase distribution of a GPC generated spot.
Supplementary Figure 3	TF-GPC allows specific two-photon photoactivation of subcellular compartments with simultaneous multiple light spots.
Supplementary Figure 4	Power dependence of ChR2 photo-depolarization in cortical brain slice.
Supplementary Figure 5	TF-GPC allows specific 2P photoactivation of neuronal compartments with simultaneous multiple light spots.
Supplementary Figure 6	Phase map computation.
Supplementary Figure 7	Spatial dependence of the 2P excitation efficiency for different methods of light patterning.
Supplementary Figure 8	Uniblitz shutter properties.
Supplementary Note 1	The Generalized Phase Contrast method: spatial dependence of diffraction efficiency and comparison with Digital Holography.

Supplementary Figure 1

Intensity distribution in GPC and DH generated light patterns.

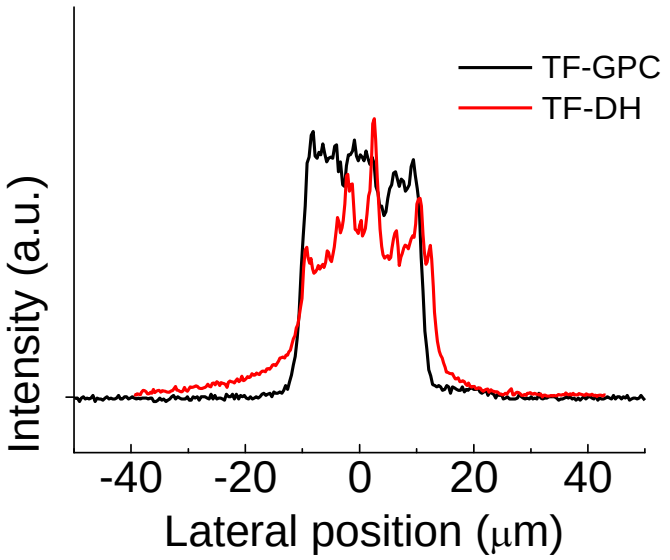

Lateral profile of the 20 μm circular spot shown in **Figure 1b** (black curve) compared to the lateral profile measured for a 20 μm circular spot generated with temporal focusing - digital holography (TF-DH) (red line) from Papagiakoumou et al.[1]. It is clear that the intensity distribution (black trace) is characterized by sharp edges and that the intensity profile is substantially homogeneous. In both of these respects, the profile is superior to what we could previously achieve in TF-DH[1], showing a less sharp cut-off at the edges and substantial speckled intensity fluctuations.

Supplementary Figure 2

Intensity and phase distribution of a GPC generated spot.

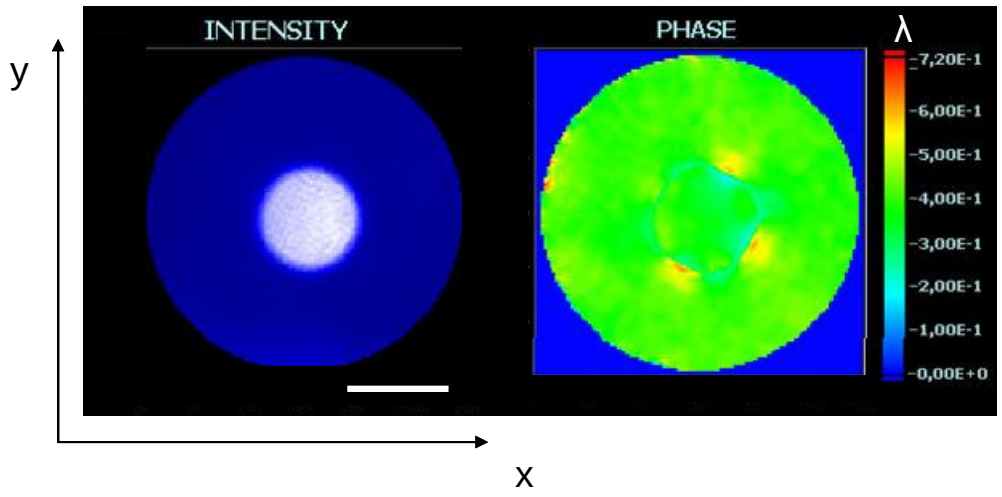

Intensity and phase distribution at the output mapping plane of the GPC system, i.e., on the grating (refer to the experimental setup illustrated in **Fig. 1a**), corresponding to a circular spot of 10 µm in diameter at the sample plane. The phase and intensity map are measured with a SID4-028 wave-front analyzer (PHASICS, S.A.). Scale bar: 1 mm.

Supplementary Figure 3

TF-GPC allows specific two-photon photoactivation of subcellular compartments with simultaneous multiple light spots.

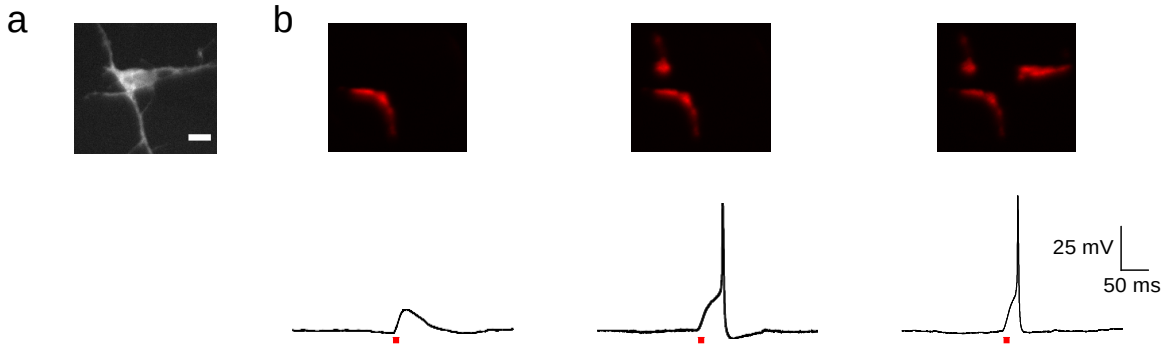

(**a**) Fluorescence image of a positive cortical neuron expressing the ChR2-H134-GFP plasmid in culture. (**b**) Excitation patterns following the dendritic morphology and corresponding photo-evoked potentials (10 ms pulses, 0.3 mW μm^{-2}). Scale bars: 20 µm; λ_{exc} = 920 nm.

Supplementary Figure 4

Power dependence of ChR2 photo-depolarization in cortical brain slices.

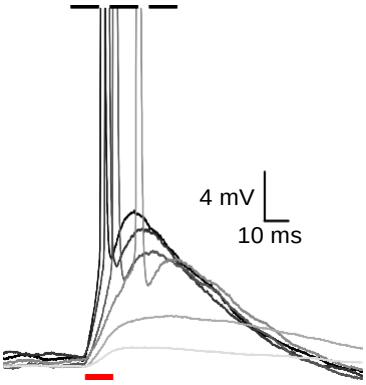

Voltage response to photo-excitation with a 10 µm light spot at increasing power density (0.10, 0.15, 0.20, 0.30, 0.40, 0.52 mW μm^{-2}, light grey to black traces) in a cortical layer V pyramidal neuron positive for ChR2. The rising phase of the photo-evoked potential becomes steeper as the excitation density increases. λ_{exc} = 920 nm.

Supplementary Figure 5

TF-GPC allows specific 2P photoactivation of neuronal compartments with simultaneous multiple light spots.

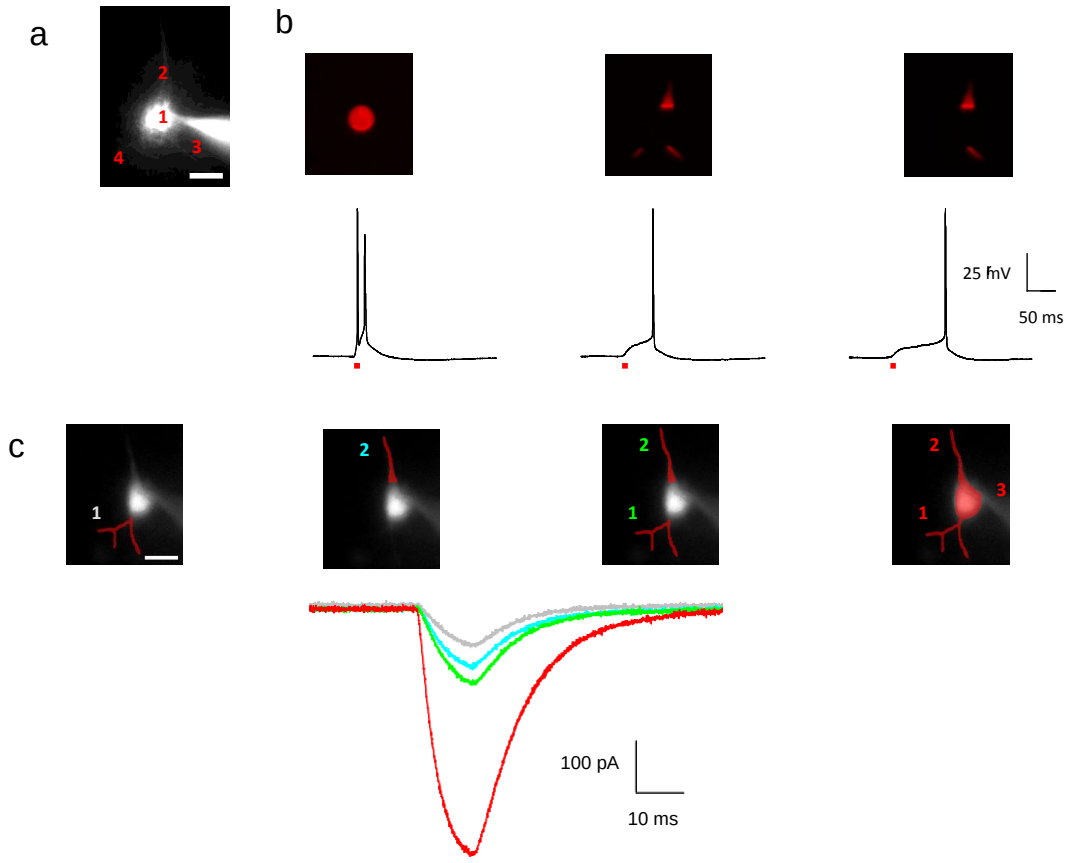

(**a**) Fluorescence image of a ChR2 positive neuron in brain slices filled with Alexa 594. (**b**) Excitation patterns (top) and corresponding photo-evoked potentials (bottom): 15 µm spot on soma (position 1), apical and basal dendrites (positions 2, 3 and 4), apical and right basal dendrite only (positions 2 and 3) (3 trials in every case, λ_{exc} = 920 nm, 10 ms pulses, 0.6 mW µm^{-2}). (**c**) Top: fluorescence image of a ChR2 positive neuron in brain slices filled with Alexa 594, with superimposed excitation patterns (red). Bottom: photo-evoked currents obtained by stimulating a basal dendrite (1, light grey), the apical dendrite (2, cyan), both apical and basal dendrite (1+2, green), apical dendrite, basal dendrite and soma (1+2+3, red) (average on 3 trials in every case, λ_{exc} = 850 nm, 10 ms pulses, 0.25 mW µm^{-2}). Scale bars: 10 µm.

Supplementary Figure 6

Phase map computation.

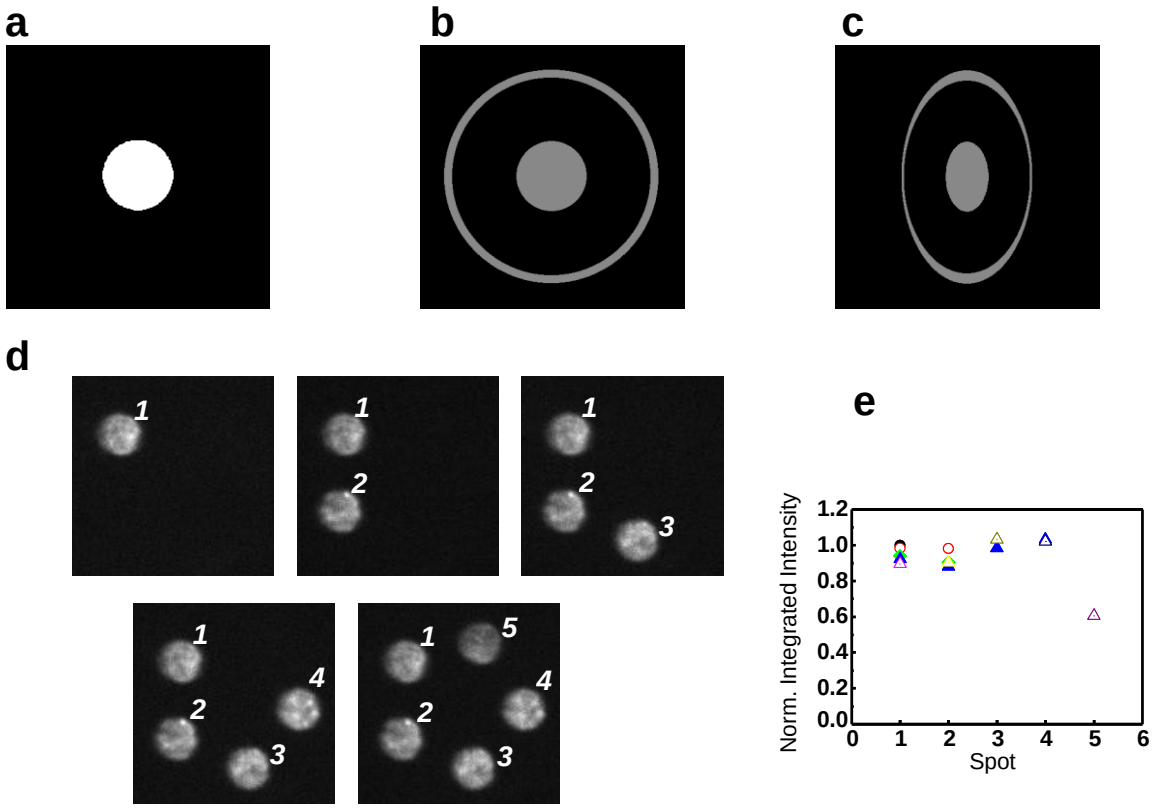

(**a**) Source image, indicating the target excitation with surface *A*(spot), at the sample plane. (**b**) Corresponding binary phase profile (the grey level of the picture corresponds to a half-wave phase shift of the applied LCOS-SLM): a ring of surface *A*(ring), is added into the phase map so that A_π(tot) = A_π(spot) + A_π(ring) is around ¼ of the illuminated area of the SLM. (**c**) Phase profile addressed to the SLM: the profile is spatially compressed along the x-direction in order to pre-compensate the stretch induced by the tilted illumination of the grating. (**d**) Series of five images of a fluorescent layer excited with one to five spots. (**e**) Integrated intensity of the spots in (**d**) showing that the excitation density within a single spot remains constant independently on the number of spots.

Supplementary Figure 7

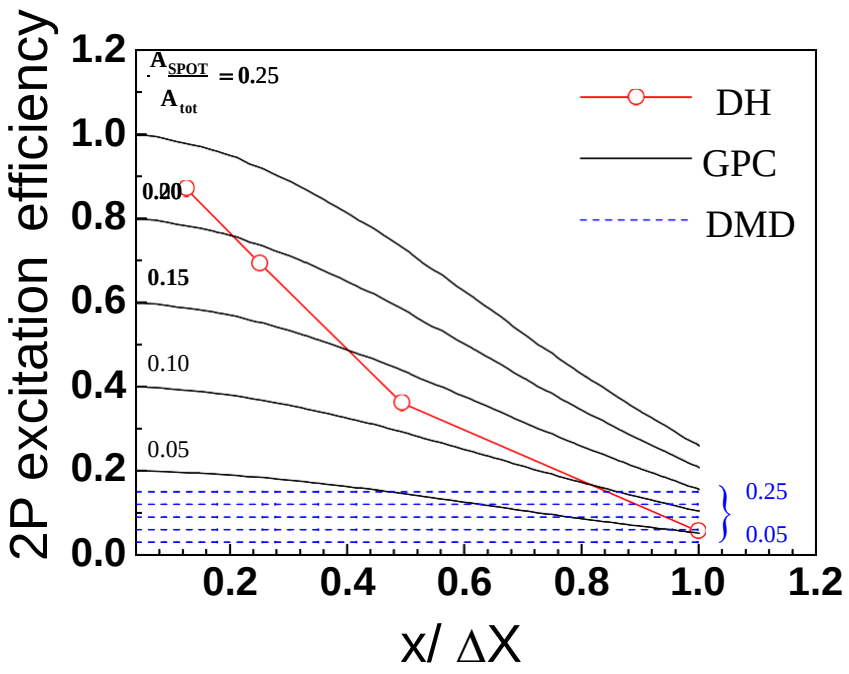

Spatial dependence of the 2P excitation efficiency for different methods of light patterning.

To take into account the quadratic dependence of 2P photoactivation on the excitation intensity, the curves are obtained as the square of the 1P curves. The black curves represent the 2P excitation efficiency for GPC, $\delta^{2P}_{GPC} = \delta_{GPC}\,(x/\Delta X)^2/\delta_{GPC}(0)$, calculated for $\eta = 0.625$[2] and for different values of the ratio A_{spot}/A_{tot}. The circular dots represent the spatial dependence of the 2P excitation efficiency for DH, $\delta^{2P}_{DH} = \delta_{DH}\,(x/\Delta X)^2/\,\delta_{DH}(0)$, based on the data from the datasheet of the LCOS-SLM (X10468-02, Hamamatsu Photonics; http://jp.hamamatsu.com/products/other/1013/1010/X10468/index_en.html). Finally, the dashed blue lines represent the excitation efficiency for a Digital Micro-mirror Device (DMD), $\delta_{DMD} = 0.61\%$ [3], multiplied to different values of the ratio A_{spot}/A_{tot}.

Supplementary Figure 8

*Uniblitz shutter properties***.**

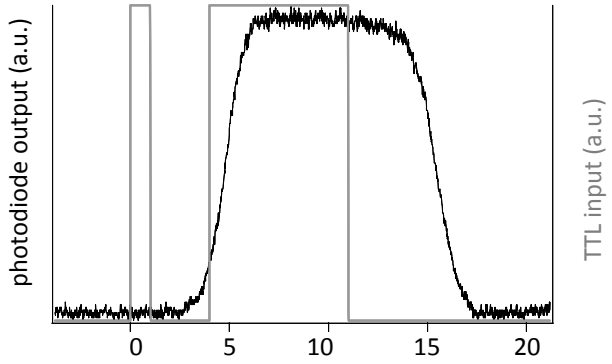

TTL input signal on the shutter (grey trace) and corresponding laser pulse measured with a photodiode at the exit of a 40×, 0.8 N.A. objective (FWHM = 10.6 ms). The shutter was opening and closing during the descending phases of two consecutive TTL signals.

Supplementary Note 1 *The Generalized Phase Contrast method: spatial dependence of diffraction efficiency and comparison with Digital Holography.*

The GPC method is based on an extension of the Zernike phase contrast approach into the domain of full-range [0, 2π] phase modulation[4]. Briefly, a desired target intensity map is converted into a spatially similar phase map that is addressed on a phase-only modulating SLM. A phase contrast filter (PCF) placed at the Fourier plane of the SLM imposes an appropriate phase retardation between the on-axis focused component and the higher-order diffracted Fourier components. The PCF is typically – but not limited to – introducing a half-wave phase shift in GPC contrary to the fixed quarter-wave phase shifting PCF of the Zernike approach. The interference between the phase-shifted focused and the scattered light, from now on referred to as the synthetic reference wave and the signal wave, respectively, allows generating a pure phase-to-intensity conversion at the output plane. To date GPC has been successfully applied in pioneering demonstrations of real-time 3D optical particle trapping and manipulation[5], wave-front sensing[6], lossless image projection[7] and phase security and encryption[8].

A crucial point to consider in the comparison between GPC and DH is the spatial dependence of the diffraction efficiency, defined as the ratio between the intensity, I_{spot}, redirected into the desired target spot(s) and the light intensity, I_{tot}, incident on the spatial phase modulating LCOS-SLM, i.e. $\delta = I_{spot}/I_{tot}$ (we neglect for simplicity the losses due to the optical elements of the light paths, as these are similar in the two methods). In DH, the diffraction efficiency, δ, depends on the LCOS-SLM pixel size, d_{SLM}, which limits the maximum spatial frequency to $f_{0max} = 1/(2d_{SLM})$. This limits the excitation field size to a square whose sides have the dimension $\Delta L = \Delta X = \Delta Y = (2\cdot\lambda\cdot f_{0max}\cdot f_1\cdot f_{obj}/f)$ [9, 10], where f_1 is the lens forming the holographic image of the target intensity and f and f_{obj} are the focal lengths of the telescope forming the replica of the output image at the focal plane of the objective. Also the number of applicable phase grey levels for the applied SLM plays an important role for the DH diffraction efficiency (for a binary-only phase SLM the highest possible theoretical diffraction efficiency is limited to 40.5%).

The diffraction efficiency, $\delta_{DH}(f_0)$, within this area depends on the spatial frequency of the hologram, f_0. For example, for the device used in this paper, holograms with a spatial frequency, f_0, comprising between 15 and 20 lpmm would generate excitation patterns with a diffraction

efficiency, $\delta_{DH}(f_0)$ encompassing between 40% and 25% of the incoming light while $\delta(f_0)$ quickly goes to zero when f_0 approaches f_{0max}, i.e. ~ 25 lpmm (**Supplementary Fig. 7**).

In general a compromise has to be found between the excitation area, the diffraction efficiency and the hologram phase resolution. Typically one can obtain A_{tot} of ~ 80 × 80 μm^2 with an overall diffraction efficiency less than 60%.

In GPC, the excitation field is typically a circular area, A_{tot}, of radius $\Delta R = \sqrt{(\Delta X^2+\Delta Y^2)} = (Rc\cdot(f_2 \cdot f_{obj})/(f_1\cdot f))$, where Rc is the radius of the circular aperture in front of the LCOS-SLM, f_1 and f_2 the focal lengths of lenses L1 and L2 of the GPC mapping system (**Fig. 1**), and f and f_{obj} are the focal lengths of the telescope forming the final intensity pattern at the objective focal plane (lens L and objective). Although for GPC it is more appropriate to talk about a phase interferometric contrasting we will keep for δ the denotation "diffraction efficiency" for similitude to the case of DH. For GPC operated in binary phase mode, two parameters determine the value of δ_{GPC} within A_{tot}. The first one is the ratio $S = A_{spot}/A_{tot}$ of the excitation pattern area, A_{spot} to A_{tot}. S can also be expressed in terms of pixel distribution at the LCOS-SLM, defined as the fill factor $F = A_\pi/(A_\pi+A_0)$, where A_π and A_0 are the number of pixels addressed with input phases π and 0, respectively. For $F = F_{max} = 0.25$ (i.e. $A_{spot} = A_{tot}/4$) the diffraction efficiency reaches a maximum value of 100% [11]. However, in the case of GPC this value decreases proportionally to $A_{spot}/A_{spot(max)}$ for areas smaller than $A_{spot(max)}$ and adjustments of the phase retardation, induced by the PCF, below π are needed for the case where A_{spot} is greater than $A_{spot(max)}$. The second parameter to be considered is the central filtering size, η, defined as the ratio between the diameter of the PCF, R_1, to the main lobe of the Airy profile of the reference wave focused at the PCF plane, R_2 - i.e. the Fourier transform of the input circular aperture of radius Rc^2.

This parameter determines the strength and the wave-front curvature of the synthetic reference wave at the GPC output aperture and therefore implicitly the diffraction efficiency of the excitation field[2]. In general a value of η between 0.5 and 0.6 represents a good compromise between wave-front curvature and strength of the synthetic reference wave, i.e. between excitation field size and intensity contrast. We can include the dependence of the diffraction efficiency on the two parameters, η and S, by defining a total diffraction efficiency for binary input phase GPC:

$\delta_{GPC} = I_{spot}/I_{tot} = \delta_\eta(r/\Delta R) \cdot 4 \cdot A_{spot}/A_{tot}$ for $A_{spot} \leq A_{tot}/4$, where r is the radius coordinate at the excitation plane and ΔR is the excitation field radius.

However, if a grey-level phase encoding is available at the input SLM of a GPC system this can be improved to show no significant spatial dependence and one can neglect the $\delta_\eta(r/\Delta R)$ term above[12].

The spatial dependence of δ_η is more flat than that of δ_{DH} (f_0) (**Supplementary Fig. 7**). However, due to the factor $A_{spot}/A_{tot,}$ the GPC overall efficiency is greater than δ_{DH} only for a limited range of spot sizes giving $A_{spot} \approx A_{spot(max)}$; for applications requiring the modification of the spot size over a broader range of values, this limitation can be overcome by using a reconfigurable beam expander that reduces the size for A_{tot}, thus compensating for the reduction in A_{spot}. However this comes at the cost of the excitation field size.

An interesting approach to be tested, can be to merge the functionalities found in optical correlators into the so-called mGPC (matched filtering GPC)[13] technique to achieve the full range of desirable light shape sizes from diffraction limited spots up to extended sized patterns. Alternatively, the advantages of DH with those of GPC, could be combined by generating excitation patterns by simultaneous control of amplitude and phase modulation[14].

Finally, Digital Micromirror-based Devices (DMDs)[3] can also be used to generate patterned photoactivation. Their main advantage is the simple optical setup and increased addressing speed. However, with these devices a large fraction of the laser power is lost because the intensity patterning is created by redirecting unwanted light out of the excitation field and into spurious higher orders. To compare this approach with DH and GPC we can also in this case define a total diffraction efficiency $\delta = I_{tot}/I_{spot}$, which results in $\delta = \delta_{DMD} \cdot A_{spot}/A_{tot}$, with $\delta_{DMD} \approx 61\%$[3] for the case of an optimal diffraction angle with a matching condition of the micro-mirror pitch, micro-mirror tilt angle and the applied wavelength of radiation – the so called Littrow configuration.

1. Papagiakoumou, E., de Sars, V., Oron, D. & Emiliani, V. Patterned two-photon illumination by spatiotemporal shaping of ultrashort pulses. Optics Express 16, 22039-22047 (2008).
2. Glückstad, J. & Mogensen, P. C. Optimal phase contrast in common-path interferometry. Appl Opt 40, 268-82 (2001).

3. Hornbeck, L. J. Digital Light Processing(TM) for high-brightness, high-resolution applications. Projection Displays Iii 3013, 27-40 238 (1997).
4. Glückstad, J. Phase contrast image synthesis. Opt.Commun 130, 225 (1996).
5. Rodrigo, P. J., Daria, V. R. & Glückstad, J. Real-time three-dimensional optical micromanipulation of multiple particles and living cells. Opt Lett 29, 2270-2 (2004).
6. Rodrigo, P. J., Palima, D. & Glückstad, J. Accurate quantitative phase imaging using generalized phase contrast. Opt Express 16, 2740-51 (2008).
7. Glückstad, J., Palima, D., Rodrigo, P. J. & Alonzo, C. A. Laser projection using generalized phase contrast. Optics Letters 32, 3281 (2007).
8. Glückstad, J. & Palima, D. Generalised Phase Contrast: Application in Optics and Photonics, 146, 310pp, Springer Series in Optical Sciences, (2009).
9. Zahid, M. et al. Holographic photolysis for multiple cell stimulation in mouse hippocampal slices. PLoS One 5, e9431 (2010).
10. Golan, L., Reutsky, I., Farah, N. & Shoham, S. Design and characteristics of holographic neural photo-stimulation systems. J Neural Eng 6, 66004 (2009).
11. Palima, D. & Glückstad, J. Multi-wavelength spatial light shaping using generalized phase contrast. Optics Express 16, 1331-1342 (2008).
12. Palima, D. & Glückstad, J. Array illumination with minimal non-uniformity based on generalized phase contrast. Optics Communications 282, 1110-1115 (2009).
13. Glückstad, J., Palima, D., Dam, J. S. & Perch-Nielsen, I. Dynamically reconfigurable multiple beam illumination based on optical correlation. Journal of Optics A-Pure and Applied Optics 11, 034012 (2009).
14. Jesacher, A., Maurer, C., Schwaighofer, A., Bernet, S. & Ritsch-Marte, M. Near-perfect hologram reconstruction with a spatial light modulator. Opt. Express 16, 2597-2603 (2008).